# PCCP

## Accepted Manuscript

Volume 18 | Number 1 | 7 January 2016 | Pages 1–636

## PCCP

Physical Chemistry Chemical Physics
www.rsc.org/pccp

ISSN 1463-9076

PERSPECTIVE
Darya Radziuk and Helmuth Möhwald
Ultrasonically treated liquid interfaces for progress in cleaning and separation processes

175 YEARS

This is an Accepted Manuscript, which has been through the Royal Society of Chemistry peer review process and has been accepted for publication.

Accepted Manuscripts are published online shortly after acceptance, before technical editing, formatting and proof reading. Using this free service, authors can make their results available to the community, in citable form, before we publish the edited article. We will replace this Accepted Manuscript with the edited and formatted Advance Article as soon as it is available.

You can find more information about Accepted Manuscripts in the author guidelines.

Please note that technical editing may introduce minor changes to the text and/or graphics, which may alter content. The journal's standard Terms & Conditions and the ethical guidelines, outlined in our author and reviewer resource centre, still apply. In no event shall the Royal Society of Chemistry be held responsible for any errors or omissions in this Accepted Manuscript or any consequences arising from the use of any information it contains.

ROYAL SOCIETY OF CHEMISTRY

rsc.li/pccp

# Evolution in Graphitic Surface Wettability with First-Principles Quantum Simulations: The Counterintuitive Role of Water

*Jin-You Lu[1], Chia-Yun Lai[1], Ibraheem Almansoori[1], Matteo Chiesa[1]\**

[1]Department of Mechanical and Materials Engineering, Masdar Institute,

Khalifa University of Science and Technology, P.O. Box 54224, Abu Dhabi, UAE

\* Address correspondence to: matteo.chiesa@ku.ac.ae

**Abstract**: Graphite surface wettability has gained a lot of interest in nanotechnology and fundamental studies alike, but what kinds of adsorption dominate its time resolved surface property variations in ambient is still elusive. Prediction of intrinsic graphite surface wettability from first-principles simulations offers an opportunity in clarifying the overall evolution. In this work, by combining experimental temporal Fourier transform infrared spectroscopy, atomic force microscopy AFM, and static contact angle measurements, with density functional theory (DFT) predicted contact angles and DFT AFM force simulations, we provide conclusive evidence that demonstrate the role that water adsorption plays in the evolution of aged graphite surface properties in ambient air. Moreover, this study has the merit of linking DFT predicted adhesive energy at solid/liquid interface and cohesive energy at liquid/liquid interface with DFT AFM predicted force of adhesion through the Young-Dupre equation. This establishes the basis

of quantum surface wettability theory by combining two independent atomic-level quantum physics simulation methodologies.

**TOC GRAPHICS**
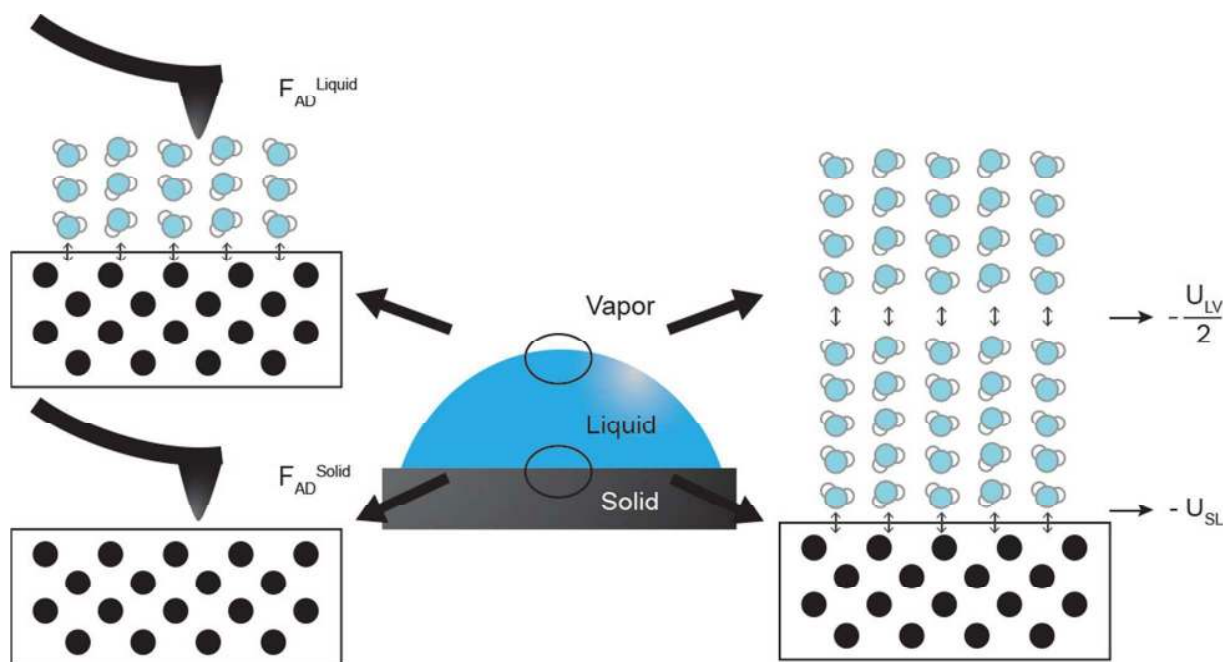


## Introduction

Thermodynamics properties such as surface energy vary as the surface exposed to the environment reach thermodynamic equilibrium and the system free energy goes towards its minimum state. As early as in 1968, experimental studies on the adsorption of different vapors contaminants on graphitized surfaces were reported[1]. Since that early study, graphite properties have been extensively exploited in several engineering fields, including the CMOS industry[2],

energy storage technology[3] and steel casting[4], to mention a few. More recently the topic of the surface properties of graphitic surfaces has gained renewed interest and one can find a many investigations that discuss the main contributors responsible for the evolution of freshly exfoliated highly oriented pyrolytic graphite (HOPG) surface towards a more hydrophobic behavior[5,6,7]. However, despite the abundant knowledge in the literature, the underlying mechanism for temporal surface property variations is still not yet fully elucidated and in particular, the role that water vapor plays is most often disregarded since this seems to contradict the hydrophobic behavior observed macroscopically. However, it is instructive to take a different look at this first few adsorbed water layers and recognize the body of evidence that demonstrates how such water layers on hexagonal surface like HOPG under ambient conditions of pressure and temperature orient in an ice-like structure, which has much different properties than are expected of water in its free phase.

In this study, highly oriented pyrolytic graphite[8] (HOPG) is employed to investigate the temporal evolution of surface property during a controlled aging process. HOPG is a periodical ABAB arrangement of two-dimensional graphene layers along the c-axis, which is stacked through van der Waals interactions. Each sheet is comprised of a hexagonal lattice of carbon bonded by strong $\sigma$ bonding ($sp^2$)) in the a-b plane (see Fig. 3(a)). We performed time resolved measurements including Fourier transform infrared spectroscopy (FTIR), static contact angle measurements, and amplitude modulation atomic force microscopy[9,10] (AM AFM) to study the evolution of graphite surface properties under ambient conditions. This temporal experimental data indicates that progressively, as clean graphite surface is exposed to the ambient air, the surface properties start to modify until equilibrium with the environment is reached. A careful comparison of the temporal experimental data indirectly points out that, when comparing

hydrocarbon contaminants and water vapor adsorption, water represents a relatively dominant factor in determining graphite surface wettability variations during the aging process. However, this conclusion is in contradiction with the reported airborne contaminant effect on the graphene[11]/graphite wettability[12] that seems to disregard the role that water and possibly its combination with hydrocarbon contaminant plays.

Therefore, we resort to quantum physics via density functional theory simulation[13] to directly evaluate how the surface wettability of graphite is influenced by pure water adsorption. We investigate this by means of a DFT-based framework developed by one of the authors that previously demonstrated to be capable of predicting macroscopic surface wettability of solid surface in contact with different liquids[14]. We predict the macroscopic surface wettability of graphite surface without inputting any experimental parameters, including water surface tensions. Moreover, we extended our computational capability by performing a rather computationally expensive DFT non-contact AFM simulations[15] on graphite surface. A silicon pyramid tip is used in order to calculate a force-distance curve comparable to what is derived from AFM measurements. The DFT predicted force profiles are able to evaluate how water adsorption influences the adhesion force and adhesion area on the graphite surface. A systematic comparison of contact angle and AFM adhesion forces between DFT simulations and experimental measurements provides a solid body of evidence that hits to how the surface wettability variations of aged graphite surface in ambient air is dominated by the first ice-like water adsorbed on the surface rather than hydrocarbon contaminants.

## Results and discussion

In Fig. 1(a), time resolved force measurements were carried out in the chamber of a Cypher AFM (Asylum Research) with standard OLYMPUS cantilevers. As the graphite surface is exposed to the ambient environment, the force measurements were performed with different aging times (*i.e.,* 0 hr, 1hr, 3hr, 6hr, 12 hr, and 24hr). Each displayed force profile for a given respective aging time step is obtained by averaging more than 1000 force curves within 15 minutes. Comparing with the fresh and aged HOPG surface force profiles, two features are noticeable owing to the surface chemistry variations: the force of adhesion $F_{ad}$ is decreased and stabilized to a constant value; as the exposure time increases, the distance of adhesion force ($A_{AD}$, AFM area) increased confirming previously presented observations[9,10].

To find which kinds of airborne contaminants play the most significant role in affecting the surface properties of HOPG in air, we performed time resolved Fourier transform infrared spectroscopy (FTIR). The FTIR measurements were carefully done by recreating the same experimental conditions of our AFM force measurements. Two major peak areas, corresponding 2800-2950 $cm^{-1}$ and 3100-3600 $cm^{-1}$,[121617] respectively, are observed in the single bond to hydrogen fingerprint region (2700-3600 $cm^{-1}$). In order to compare the FTIR spectra with different aging times, each measured spectrum was normalized by the most intense peak (~2950 $cm^{-1}$). The major peak at 2850 $cm^{-1}$ and 2950 $cm^{-1}$ is recognized as C-H bonds stretching (Alkanes functional class), which is a response to hydrocarbon contamination possibly adsorbed from air[12,17]. However, a broad peak area at 3100-3400 $cm^{-1}$ corresponding to the O-H bonds stretching[18], which is neglected in previous discussions[6,1,2,19], relatively increases as the aging time increases. The O-H bonds with the band center at 3250 $cm^{-1}$ corresponds to the completed hydrogen bonding network of the ice-like water adlayer on graphite surface[7]. Another peak, at 3350-3400 $cm^{-1}$, on the shoulder of broad O-H band comes from the signal of liquid water[20].

Both AFM adhesion area and FITR O-H stretching integration areas increase with increasing the aging time. As a consequence of these observations, we speculate that as the graphite sample is exposed to the ambient air, gradually increased surface-bonded water molecules are formed on the graphite surface, which relatively dominate the graphite surface chemistry. With the evidence provided by AFM and FTIR, see Figure 1, one cannot disregard the role played by hydrocarbon contaminants, but one needs to recognize the role that adsorbed water plays. Despite attempting exfoliating the HOPG in hydrocarbon free environments, the exposure to air during the transfer to the FTIR experiment does not provide conclusively evidence that suggest disregarding airborne hydrocarbon.
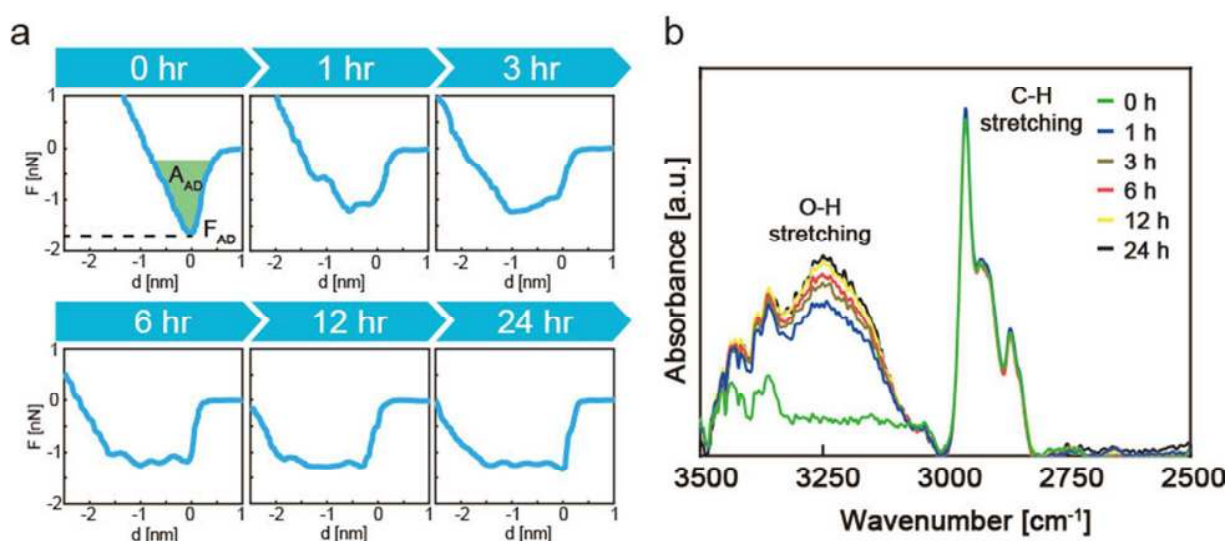


Figure 1. (a) AFM force profiles on aged graphite surfaces with different aging times. (i.e. 0 hr, 1hr, 3hr, 6hr, 12 hr, and 24hr). (b) Time resolved FTIR spectroscopic measurements on graphite surface with different aging times.

We then revert to a computational framework whose graphitic surface condition can be predefined at request. We computationally evaluate how the water adsorption affects the graphite surface without the presence of hydrocarbons. We perform state of the art van der Waals density-functional theory simulation ((i.e. vdW-DF2-C09 (2010)[21], which is considered to have a better

energy prediction of graphite system[22], to study multiple water layers on graphite surface. The adsorption energy per water molecule $U_{ad}^m$ of the $m^{th}$ water layer on the graphite surface covered with ($m$-1) water layers is calculated by means of Eq. (1),

$$U_{ad}^m = \frac{U_{S+mL} - U_{S+(m-1)L} - U_{mL}}{n_L}, U_{ad}^{m=1} = U_{SL}; U_{ad}^{m\ ^1} \cong \frac{U_{LV}}{2} \tag{1}$$

where $U_{S+mL}$ is the total energy of a graphite surface with $m^{th}$ ice-like water layers above the surface, $U_{S+(m-1)L}$ is the total energy of a graphite surface with ($m$-1) overlaying water layers, $U_{mL}$ is the total energy of the $m^{th}$ water monolayer, and $n_L$ is the number of molecules in one water monolayer, which is eight in our DFT simulation domain. Our computational framework[14] allows us to extract the adhesion energy $-U_{SL}$ at the water/graphite interface and cohesion energy $-U_{LV}/2$ at water/water interface from DFT calculated adsorption energy studies.as shown in the Fig. 2(a). The details behind our computational simulations are included in the section of computational details.

The water/graphite configuration used in the DFT simulation is multiple ice-like water layers on graphite surface, as shown in Fig. 2(a). Detailed discussion on the configuration of water on graphite surface is included in Section SI of Supporting Information. The top view of water on graphite is shown in Fig. S1(e). It is generally observed that in ambient air, the first water adlayer on HOPG surface is an ice-like water layer[23,24]. Once the adhesive energy $U_{ad}^{m=1} = U_{SL}$ at the graphite/water interface is obtained, we keep adding other ice-like water layers on top of water covering graphite surface in order to calculate the cohesive energy between two water layers. The number of ice-like water layers is increased gradually (one water layer at a time) up to seven layers, and the cohesive energy is obtained by the convergence of adsorption energy studies in Fig. 2(b), which means that the cohesive energy is no longer influenced by the

graphite surface. The predicted adhesive energy $U_{ad}^{m=1} = U_{SL}$ is larger than the cohesive energy $U_{ad}^{m>1}$ between water layers, this yields the water contact angle on graphite to be less than 90°. The total energy $U_{mL}$ of the individual $m^{th}$ water monolayer is summarized in the Fig. S1(b). This water/graphite configuration is definitely not the same as the bulk water droplet on graphite surface on the atomic scale, but the average cohesive energy between two ice-like water layers above the solid surface should be close to that of bulk water. The reason is that the interfacial tensions of water and ice are close to each other (water: 72.8 mN/m; ice water: 75.6 mN/m).

For completeness sake, we study graphite with different number of graphene layers in a ABAB stacking, as shown in Fig. 2(b). For graphite with more than one layer of graphene, the positions of carbon atoms in the bottom layer of graphite were fixed to represent the bulk sites during the DFT geometry relaxation calculations. As the number of graphite layers is increased, the adsorption energy per water molecule of the first water layer on graphite surface gradually converges. Comparing the graphite surfaces with four and five graphene layers, the difference of their adsorption energies per water molecule at first water layer on different graphite surfaces is negligible (<0.1 KJ/mol). Finally, the adhesion energy $U_{SL}$ was obtained by taking the adsorption energy per water molecule of the first water layers (m=1) on the graphite surface. The sharp drop of adsorption energy on water-wet graphite surfaces happened in some cases, which are possibly related to the interaction distance between graphite surface and water molecules. The distance of fifth water layer on graphite surface is 16.5 Å, which is larger than the binding distance of vdW-DF2 functional for the description of the interaction between molecule and graphene surface around 14 Å [25]. The adsorption energy of higher water layer than fourth layer belong to pure interaction between water and water layers, and thus a drop of cohesion energy is possibly observed. Therefore, the cohesion energy $-U_{LV}/2$ was obtained by averaging the adsorption

energies per water molecule of the water layers (m=5~7) above four layers, which is considered to be close to bulk water. Then, figure 2(c) shows that the water contact angles on graphite with different number of graphene layers are predicted based on the Young-Dupre equation, as given by.

$$\cos(\theta) = \frac{U_{SL} - U_{LV}/2}{U_{LV}/2} \tag{2}$$

and where the energy $U_i$ are obtained numerically.

It should be noted that our simulation results are determined by pure DFT total energy studies on water/graphite surface without inputting any experimental.
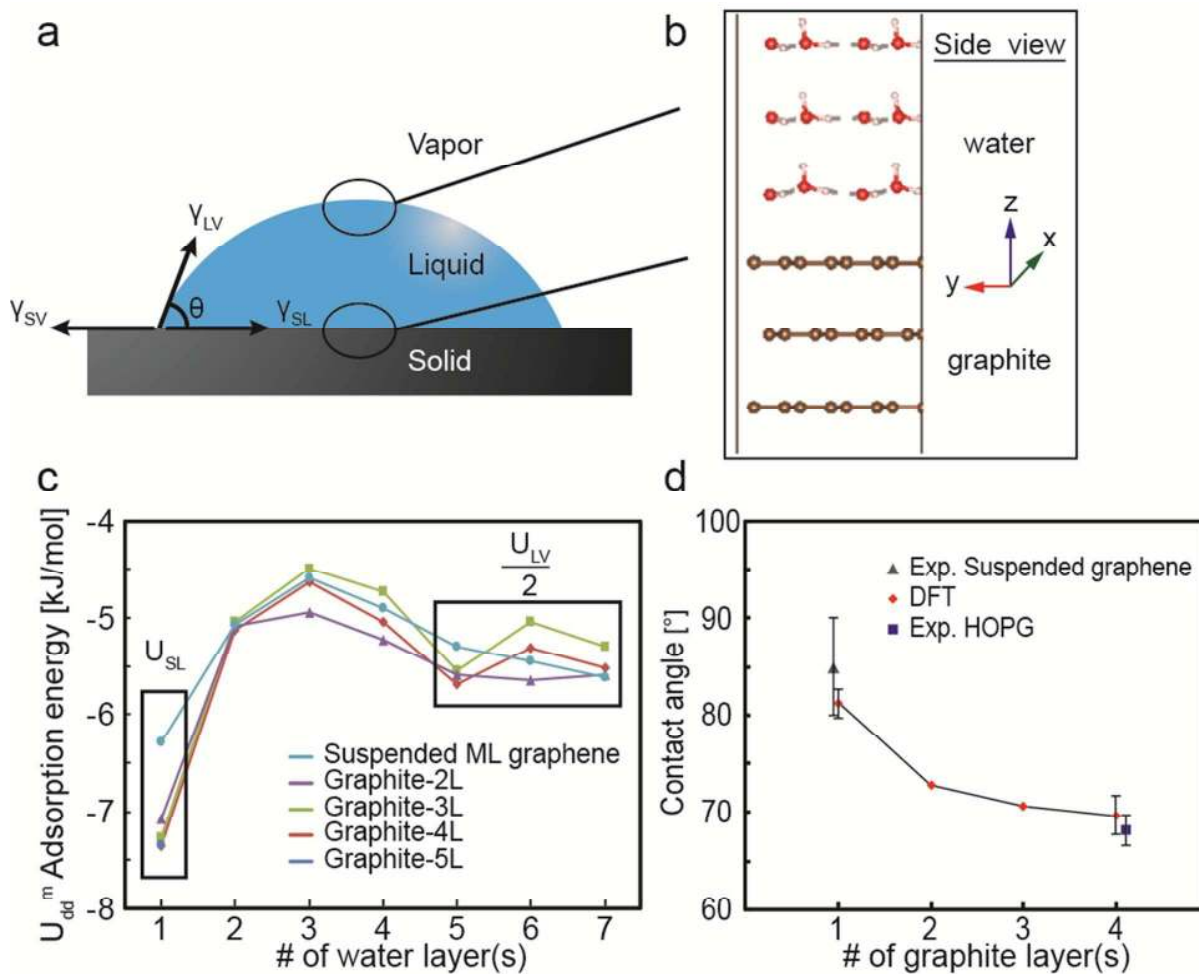
Figure 2. (a) Schematic diagram to predict the surface wettability of a solid by a liquid. The adhesion energy at the solid/liquid interface and the cohesive energy at liquid/vapor interface can be predicted with the DFT solid/liquid slab model. (b) configuration of multiple ice-like layers on graphite surface in the DFT simulation domain. Each water layer consists of eight $H_2O$ molecules, and a water molecule consists of two white hydrogen atoms and one red oxygen atom. Each graphene layer has thirty-two carbon atoms. (c) the adsorption energy per water molecule at different ice-like water layers on fresh graphite surface. Graphite surface with different number of graphene layers from one to five is also presented. (d) DFT predicted water contact angles on graphite with different number of graphene layers.

The predicted contact angles of water droplet on graphite and suspended monolayer graphene agree well with the published experimental static contact angles see ref[26], respectively, as summarized in Table 1. The uncertainty of DFT predicted contact angle in Table 1 comes from the standard deviation of cohesion energy, which is 0.31 kJ/mol. In addition to the predicted results with using vdW-DF2-C09, we also included the simulation results of water on graphite surface by using another van der Waals functional vdW-DF2[27] based on the same configurations, which predicts similar trend as vdW-DF2-C09 did but gives higher water contact angle owing to overestimation of hydrogen binding among water molecules. One major advantage of our DFT contact angles prediction is that the graphite surface is clean without any presence of hydrocarbon contaminants from the ambient air. The agreement between DFT prediction and experimental contact angles seems to conclusively indicate that hydrocarbon contaminants on graphite surface wettability play at most a secondary role in determining wettability.

According to the AFM and FTIR measurements, the water layers are gradually adsorbed on the graphite surface when increasing the aging time. If the binding between water and graphite surface is strongly formed, the top bulk water would mainly interact with the water

adsorbed on graphite surface rather than pure graphite. Therefore, when graphite surface is aged, the predicted adhesion energy $-U_{SL}$ in our DFT surface wettability methodology is changed from $U_{ad}^{m=1}$ to $U_{ad}^{m>1}$. This infers bulk water interacting with water overlaying graphite surface as the surface water layers is formed, as illustrated in Fig. 3(a). Subsequently, we compare the DFT-predicted water contact angles on water overlaying graphite surface to the time resolved experimental stable contact angles, as shown in Fig. 3(b). Agreement between predicted and measured surface wettability when the graphite surface is clean, yields a less hydrophobic behavior. Once the graphite is aged, the contact angle shifts towards a more hydrophobic behavior. This prediction explains why once the solid surfaces such as oxides[28], calcite[29], and mica[30] surfaces, are exposed in ambient air, the aged solid surfaces have increasingly larger water contact angle.

Table 1. A comparison between the predicted and experimentally measured water droplet on graphite/graphene surfaces

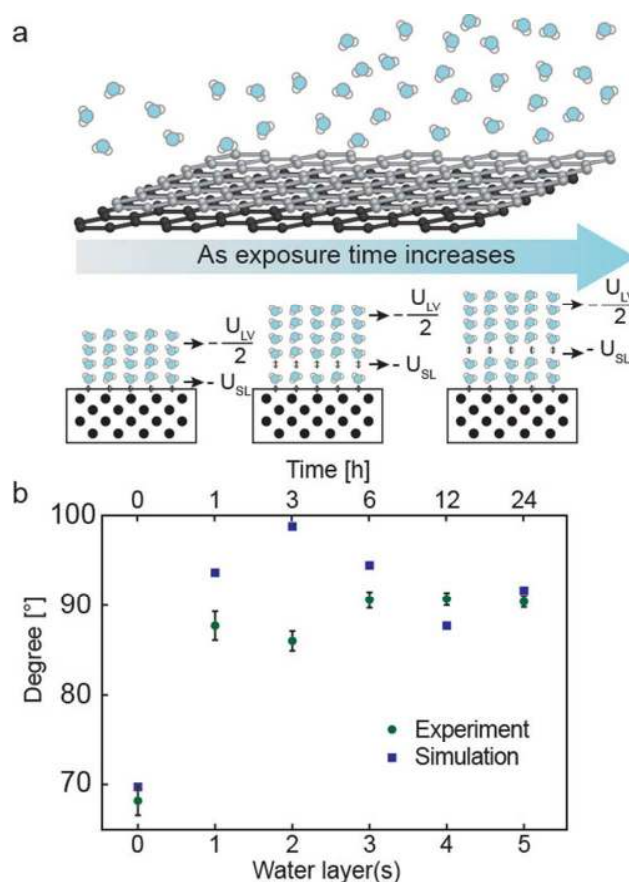| Solid surface | $U_{LV}/2$ [KJ/mol] | $U_{LV}/2$ [KJ/mol] | DFT $\theta$ | Exp. $\theta$ |
|---|---|---|---|---|
| Suspended graphene | 6.29 | $5.46 \pm 3.1$ | $81.3°\pm 3.7°$ | $85° \pm 5°$[26] |
| graphite | 7.36 | $5.46 \pm 3.1$ | $69.7°\pm 4.8°$ | $68.2° \pm 1.6°$ |

Figure 3. (a) Time resolved schematic of water adsorption on graphite surface under ambient environment. (b) Comparison of time resolved DFT predicted water contact angles on graphite surface with different number of water layer adsorption and experimentally measured static contact angles with different aging times.

The surface energy of aged graphite surface is reduced owing to the strong binding between the first water monolayers and graphite. This comes as a consequence of our temporal contact angle prediction based on experimental FTIR and AFM data. In order to further support this point, we performed computationally-expensive noncontact AFM scanning DFT simulation with a pyramid silicon tip ($Si_{10}H_{15}$) on graphite surface to obtain a direct comparison with the experimental force profiles. The water/graphite surface consist of two layers of graphene in a AB stacking and one ice-like water layer above the graphite surface. The predicted force profiles are taken from the gradient of total energy of the tip-surface system, which is given by

$F = -\nabla(E_{tot}(d))$. Before running noncontact atomic force simulations, the silicon pyramid tip ($Si_{10}H_{15}$), graphite surface, and graphite surface with one monolayer ice-like water are, respectively, relaxed by performing DFT geometry optimization[31]. The silicon tip is approached towards the carbon atom of the graphene with a quasi-static interval of 0.2 Å in each step of AFM-like scanning, as shown in Fig. 4(a). During DFT AFM scanning, the positions of silicon pyramid tip ($Si_{10}H_{15}$) are fixed except that of the four silicon atoms at the tip apex that are allowed to relax. Meanwhile, the bottom layer of graphite is also fixed to represent the bulk sites. Two different cases of graphite with fixed ice-like water layer and free ice-like water layer are discussed in order to distinguish possible chemical reactions caused by the interaction between silicon tip and water molecules.

The comparison of DFT predicted force profiles on graphite surface and graphite surface with fixed one ice-like water layer are shows in Fig. 4(a). Once the water is adsorbed on the graphite surface, the force of adhesion $F_{ad}$ is decreased. This captures the experimentally observed reduced force of adhesion $F_{ad}$ on aged graphite surface. Although the fixed water molecules on graphite surface in the DFT simulations are definitely not realistic in the ambient conditions, it significantly reduces computational time and avoids possible chemical reactions between silicon tip and water molecules during the scanning.

The DFT predicted force profile on graphite with free ice-like water layer gives a better agreement of adhesion force and adhesion area with the experimental data, as shown in Fig. 4(b). However, a sudden drop happened in the simulated repulsive force region, which corresponds to bonding between the O-H and the silicon tip, as shown in the inset of Fig. 4(a). The stability of current used silicon tip may influence the interaction force values[32,33]; however, the DFT

predicted force of adhesion $F_{ad}$ is still valid because the chemical reaction between the silicon tip and water molecules happened after reaching the point of force of adhesion. The DFT predicted force curves in Fig. 4(a) corresponds to the scanning at the position on the top of graphene's carbon atom in a quasi-static manner from top to bottom. In order to capture the overall picture, we also probe another point (Site B) on the centre of the graphene hexagon, as compared to the point (Site A) on the top of graphene's carbon atom in Fig. 4(c). The drop owing to the OH-bonded to silicon tip is captured earlier in the force-distance curve on site B, as shown in Fig. 4(d). We found that as tip moves closer to the surface, this bonding inevitably happen and the position of the large attractive force drop in the force-distance is dependent on the distance between the tip apex and nearest water molecules.
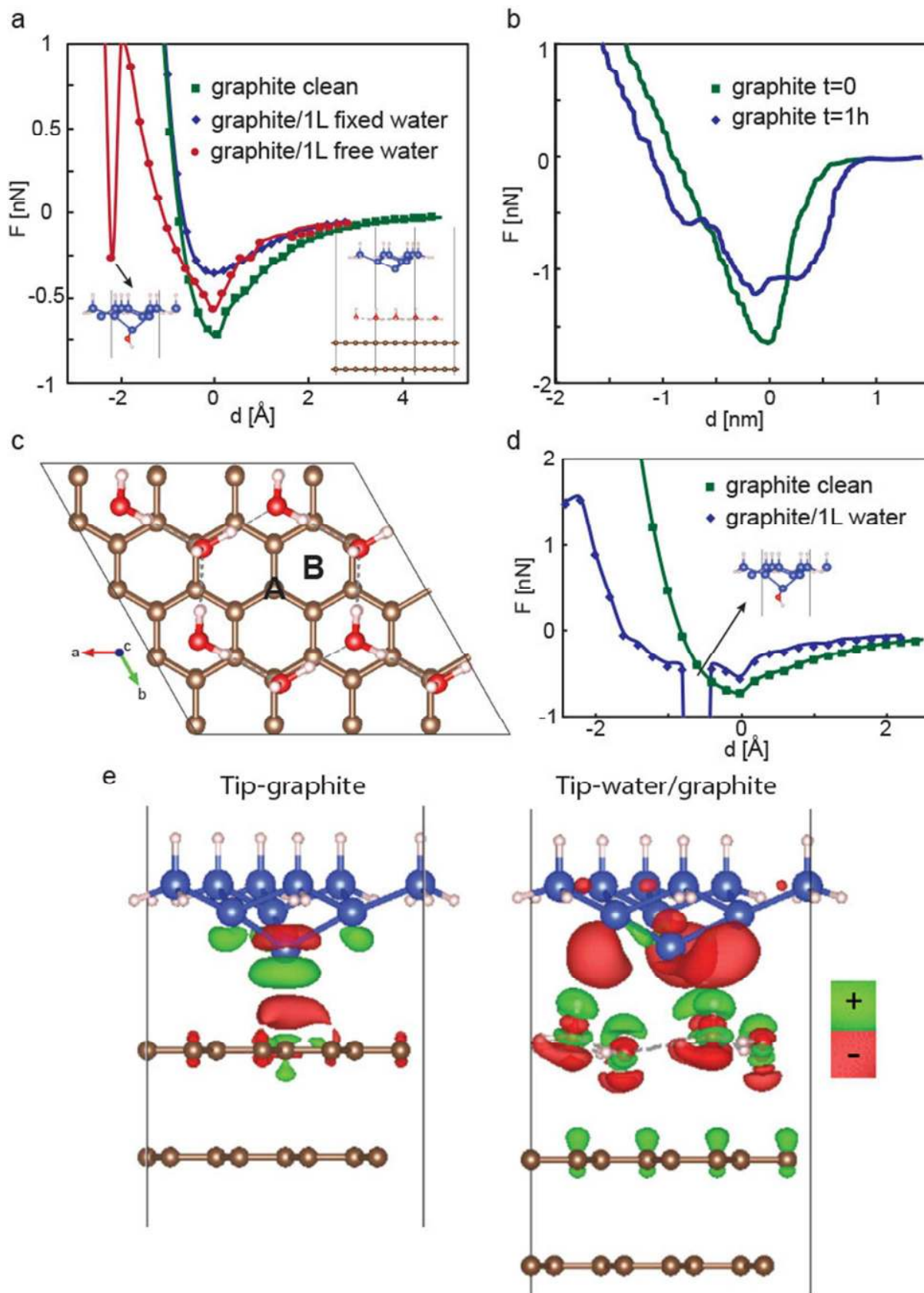
Figure 4. (a) DFT predicted force profiles on graphite surface with and without one ice-like water adsorption above the surface. The silicon pyramid tip consists of ten blue silicon atoms and fifteen white hydrogen atoms. An inset of OH-bonded silicon tip appeared in the simulated repulsive region. (b) AFM force profiles on fresh and one-hour aged graphite surface in ambient conditions. (c) site A corresponds to the point at the top of carbon atoms, and site B corresponds to the center of the graphene hexagon. (d) DFT predicted force profiles on probing site B of the graphite and water/graphite surfaces. (e) Comparison of the charge density difference distributions between silicon tip to graphite surface and silicon tip to water/graphite surface.

However, if in first approximation, the chemical reactions between water and silicon tip is ignored in the DFT force simulations, we just focus on the magnitude of predicted forces of adhesion $F_{ad}$. An alternative way to predict the macroscopic surface wettability (*i.e.* contact angle) can be proposed based on DFT noncontact AFM simulations. The predicted forces of adhesion $F_{ad}$ on graphite and water overlaying graphite are directly proportional to the work of adhesion per unit area of graphite and water layer, respectively[34][35]. Through Young-Dupre equation, the contact angle of water droplet on graphite surface can be predicted by the following equation

$$\cos(\theta) = \frac{W_{SL} - \gamma_{LV}}{\gamma_{LV}} \approx \frac{F_{ad}^{G} - F_{ad}^{W/G}}{F_{ad}^{W/G}} \tag{3}$$

Where $F_{ad}^{G}$ and $F_{ad}^{W/G}$ are the forces of adhesion on graphite and water/graphite surfaces, respectively.

This equation is valid when the solid substrate effect is negligible and the chemical reactions between silicon tip and liquid molecules are ignored. The agreement between the predicted and experimental contact angles, is summarized in Table 2, this demonstrates the efficacy of this DFT-AFM contact angle prediction methodology. A detailed derivation of Eq. (3) is discussed in the Section III of Supporting Information. Meanwhile, the Young-Dupre equation can also be

expressed in terms of adhesion (binding) energy $U_{ad}$ between silicon tip and surfaces, as shown in Fig. S4. Both adhesion energy and force of adhesion calculated by DFT-AFM simulations gives similar prediction of graphite surface wettability, as summarized in Table S1. Agreement between contact angles predicted by DFT-AFM adhesion energy and DFT-AFM force of adhesion provide a self-consistent evidence of our DFT numerical AFM experiment.

The charge density difference distributions of the silicon tip to surface system with and without the monolayer of water further provides physical insights into the interaction between silicon tip and surfaces, as illustrated in Fig. 4(e). We simulated the tip/surface systems and derive the force of adhesion where the largest attractive force between silicon tip and surfaces occurs in the force-distance curve. Aptly named, the charge density difference distribution requires three calculations of charge densities including tip, surface, and tip/surface systems to explore the effect of the binding between the silicon tip and probing surface on electrostatic charge distribution. A quite different charge density distribution near the silicon tip apex in these two systems is observed. Meanwhile, the electrostatic interaction between water dipoles and silicon tip apex is larger than that of graphene and silicon tip owing to the significantly polarized charges between water dipoles and silicon tip apex. However, when it comes to compare the DFT predicted and experimental force profiles of graphite and water/graphite surfaces, the force adhesion of silicon tip to clean graphite surface is larger. This difference originates from the fact that the silicon tip interacts with graphite surface mainly through the van der Waals-London dispersion (nonpolar) forces while the silicon tip interacts with water molecules mainly through (polar) acid/base forces, as indicated by the polarized charges on the interacting surfaces in Fig.4(e).

In this work, the graphene/graphite surface wettability is predicted based on the proposed ice-like structure of the water layers on graphite with standard DFT simulations, which are effectively at zero temperature. As the temperature effect is included, both the adhesion energy at the solid/liquid interface and cohesion energy at the liquid/liquid interface are decreased owing to the thermal motions of molecules, which causes the adsorption energy of water molecules to be decreased. Computationally expensive ab initio molecular dynamics simulations of a liquid/solid system are required to perform at different temperatures for a long period of time in order to obtain the dependence of temperature on adhesion and cohesion energies. For water on graphite, the change of contact angle with increasing environmental temperature should be less because the magnitude of adhesion and cohesion energy are close. Therefore, the contact angles predicted by the density functional theory simulations agrees well with the static contact angle measured at the room temperature.

Table 2. A comparison of contact angle prediction based on the DFT predicted and experimentally measured force of adhesion

| Graphite surface | $F_{ad}^{graphite}$ (nN) | $F_{ad}^{water}$ (nN) | Contact angle θ (°) | Experimental static contact angle (°) |
|---|---|---|---|---|
| DFT-AFM | -0.720 | -0.552 | $72.3^{\circ}$ | $68.2^{\circ} \pm 1.6^{\circ}$ |
| AFM | -1.69 | -1.26 | $70^{\circ}$ | |

In summary, a time resolved FTIR spectroscopic study on graphite surface conclusively shows that in the ambient environment, the adsorbed water molecules are relatively increased as compared to adsorbed hydrocarbon contaminants during the aging process. By evaluating the water adsorption on graphite surface, the DFT predicted contact angles and AFM force profiles

agrees and seem to explain the time resolved evolution of experimental contact angle and force measurements on aged graphite surface. This agreement demonstrates that water adsorption is the major factor in affecting the surface energy (surface wettability) of aged graphite surfaces.

In the past one century, numerous contact angle measurements of solid surface for different liquids have been reported to evaluate the surface wettability. However, the water adsorption itself (or aging effect) is usually disregarded in the discussion. Our studies point out that the binding between graphite surface and water vapor from the ambient environment is able to solely yield the graphite surface to become more hydrophobic. This finding not only provide a deep insight into the graphite and graphene wettability, but also can be applied to other different solid surfaces. Meanwhile, we successfully link the DFT-AFM predicted force of adhesion with the methodology of DFT contact angle prediction. Therefore, the basis of quantum wettability simulations is established by combining two independent ab-Initio quantum simulation methodologies with Young-Dupre equation.

# Material and methods

### Sample preparation

Highly Ordered Pyrolytic Graphite (HOPG) is used for its flatness that makes it possible to disregard any morphological effect and easy to create a new surface when studying the evolution of surface properties. We used scotch tape method to create a pristine surface that is immediately exposed to ambient conditions for water contact angle and atomic force microscopy study, and a controlled $N_2$ environment at 1220 Pa for FTIR study (Temperature at $23\pm2°C$ and relative humidity (RH) ~$55\pm5\%$).

### Diffuse Reflectance Infrared Fourier Transform Spectroscopy DRIFT-FTIR

Using a Praying Mantis Diffuse Reflection Accessory, we mounted the HVC-DRP reaction chamber (from Harrick Scientific) in the front sample compartment of a Bruker 80v FTIR spectrometer. The controlled environment in the reaction chamber is connected to a Netzsch drop humidity generator and a $N_2$ gas cylinder by a mass flow meter. Heat transfer lines are used to connected different instruments allowing the whole system to be maintained at constant temperature. Immediately after cleaving (cr. 3 minutes), the pristine HOPG surface is placed in the reaction chamber and reflects the IR beam while being exposed to a predefined environment. Time 0 refers to the start of a cycle when the sample is just mounted in the experimental set up and is exposed to the humid $N_2$ gas (no water adsorbed). Throughout this work, the temperature for the transfer lines and the reaction chamber is kept at 42°C. We record the absorbance spectrum every 10 min in reflective mode by averaging 150 scans with a resolution of 4 cm$^{-1}$.

**Force measurement**

We used the Cypher AFM from Asylum Research and operated in amplitude modulation (AM) mode. Standard OLYMPUS cantilevers (AC160TS) were used and the specifications of the cantilever are k (spring constant) $\approx$ 30 N/m, $f_0$ (natural frequency) $\approx$ 250 kHz, and Q $\approx$ 300. We recorded the raw amplitude A and phase $\varphi$ versus separation distance (d) curves, and exploited Sader-Jarvis-Katan formalism[363738] to reconstruct the force. To avoid bistability, free cantilever oscillation amplitudes of 60 nm were used to record the amplitude-phase-distance curves. Also, it is known that the AFM tip radius R plays an important role in the reconstructed force, we ensured R remained constant throughout the experiment with critical amplitude method *in situ*[39]. For each time step, a total of 150 AFM curves were recorded for statistical analysis.

**Contact angle measurement**

The SCA measurements were conducted at 22°C and 55% RH with a Krüss FM40Mk2 EasyDrop contact angle instrument. We recorded the images of the water droplets with the Stingray CCD and data analysis was processed with the standard software supplied by Krüss. SCA was measured using 2 μL droplets and statistics referred to 10 measurements for each time step.

**Computational details**

**Density functional theory surface wettability simulations.** We use van der Waals density functional with the Cooper's exchange (vdW-DF2$^{C09}$) to perform total energy studies of multiple ice-like water layers on graphite surface. All DFT simulations of multiple ice-like layers on graphite surface were performed using the Quantum Espresso package[13]. The kinetic energy cutoffs and density cutoffs are set as 45/450 Ry with 3x3x1 Monkhorst-Pack k-point mesh[40] for all the total energy calculations. The criterion for the geometry optimization is met once the total energy is less than $1 \times 10^{-4}$ Ry and the interatomic force is less than $1 \times 10^{-3}$ Ry/bohr.

**Density functional theory noncontact atomic force simulations**. All DFT noncontact atomic force simulations were performed using the Quantum Espresso package[13]. The potential basis sets in the generalized gradient approximations (GGA) use Perdew Burke Ernzerhof[41] (PBE) functional and ultra-soft pseudopotentials. For van der Waals corrections, the DFT-D2 method of Grimme [42] is applied to DFT simulations. The reason for using PBE ultra-soft pseudopotential and DFT-D2 rather than density functional with the Cooper's exchange is to save the computational efforts. The kinetic energy cutoffs and density cutoffs are set as 35/350 Ry with 3x3x1 Monkhorst-Pack k-point mesh[40] for all the AFM scanning calculations. Silicon pyramid tip ($Si_{10}H_{15}$) and graphite surface comprising of multilayer graphene in a ABAB-stacking are relaxed by performing DFT geometry optimization, respectively, before running DFT noncontact

atomic force simulations. The criterion for the geometry optimization is met once the total energy is less than $1 \times 10^{-4}$ Ry and the interatomic force is less than $4 \times 10^{-4}$ Ry/bohr. The force profiles are directly extracted by taking the gradient of the total energy of the system versus the distance between the silicon tip and solid surface.

## ACKNOWLEDGMENT

## REFERENCES

(1)    Belyakova, L. D.; Kiselev, A.V; Kovaleva, N.V.Gas-Chromatographic Determination of Isotherms and Heats of Adsorption of Water Benzene and Methanol Vapours on Graphitised Carbon Black. *Russ. J. Phys. Chem.* **1968**, *42* (9), 1204–+.

(2)    Ramón, M. E.; Gupta, A.; Corbet, C.; Ferrer, D. A.; Movva, H. C. P.; Carpenter, G.; Colombo, L.; Bourianoff, G.; Doczy, M.; Akinwande, D.CMOS-Compatible Synthesis of Large-Area, High-Mobility Graphene by Chemical Vapor Deposition of Acetylene on Cobalt Thin Films. *ACS Nano* **2011**, *5* (9), 7198–7204.

(3)    Karaipekli, A.; Sarı, A.; Kaygusuz, K.Thermal Conductivity Improvement of Stearic Acid Using Expanded Graphite and Carbon Fiber for Energy Storage Applications. *Renew. Energy* **2007**, *32* (13), 2201–2210.

(4)     Li, Y.; Chen, X.Microstructure and Mechanical Properties of Austempered High Silicon

        Cast Steel. *Mater. Sci. Eng. A* **2001**, *308* (1–2), 277–282.

(5)     Mücksch, C.; Rösch, C.; Müller− Renno, C.; Ziegler, C.; Urbassek, H. M.Consequences

        of Hydrocarbon Contamination for Wettability and Protein Adsorption on Graphite

        Surfaces. *J. Phys. Chem. C* **2015**, *119* (22), 12496–12501.

(6)     Kozbial, A.; Li, Z.; Sun, J.; Gong, X.; Zhou, F.; Wang, Y.; Xu, H.; Liu, H.; Li,

        L.Understanding the Intrinsic Water Wettability of Graphite. *Carbon N. Y.* **2014**, *74*, 218–

        225.

(7)     Li, Z.; Kozbial, A.; Nioradze, N.; Parobek, D.; Shenoy, G. J.; Salim, M.; Amemiya, S.; Li,

        L.; Liu, H.Water Protects Graphitic Surface from Airborne Hydrocarbon Contamination.

        *ACS Nano* **2015**, *10* (1), 349–359.

(8)     Chang, H.; Bard, A. J.Observation and Characterization by Scanning Tunneling

        Microscopy of Structures Generated by Cleaving Highly Oriented Pyrolytic Graphite.

        *Langmuir* **1991**, *7* (6), 1143–1153.

(9)     Amadei, C. A.; Lai, C.-Y.; Heskes, D.; Chiesa, M.Time Dependent Wettability of

        Graphite upon Ambient Exposure: The Role of Water Adsorption. *J. Chem. Phys.* **2014**,

        *141* (8), 84709.

(10)    Lai, C.-Y.; Tang, T.-C.; Amadei, C. A.; Marsden, A. J.; Verdaguer, A.; Wilson, N.; Chiesa,

        M.A Nanoscopic Approach to Studying Evolution in Graphene Wettability. *Carbon N. Y.*

        **2014**, *80*, 784–792.

(11)    Rafiee, J.; Mi, X.; Gullapalli, H.; Thomas, A.V; Yavari, F.; Shi, Y.; Ajayan, P. M.; Koratkar, N. A.Wetting Transparency of Graphene. *Nat. Mater.* **2012**, *11* (3), 217.

(12)    Li, Z.; Wang, Y.; Kozbial, A.; Shenoy, G.; Zhou, F.; McGinley, R.; Ireland, P.; Morganstein, B.; Kunkel, A.; Surwade, S. P.Effect of Airborne Contaminants on the Wettability of Supported Graphene and Graphite. *Nat. Mater.* **2013**, *12* (10), 925.

(13)    Giannozzi, P.; Andreussi, O.; Brumme, T.; Bunau, O.; Nardelli, M. B.; Calandra, M.; Car, R.; Cavazzoni, C.; Ceresoli, D.; Cococcioni, M.Advanced Capabilities for Materials Modelling with Quantum ESPRESSO. *J. Phys. Condens. Matter* **2017**, *29* (46), 465901.

(14)    Lu, J. Y.; Ge, Q.; Li, H.; Raza, A.; Zhang, T.Direct Prediction of Calcite Surface Wettability with First-Principles Quantum Simulation. *J. Phys. Chem. Lett.* **2017**, *8* (21), 5309–5316.

(15)    Pérez, R.; Štich, I.; Payne, M. C.; Terakura, K.Surface-Tip Interactions in Noncontact Atomic-Force Microscopy on Reactive Surfaces: Si (111). *Phys. Rev. B* **1998**, *58* (16), 10835.

(16)    Snyder, R. G.; Hsu, S. L.; Krimm, S.Vibrational Spectra in the C   H Stretching Region and the Structure of the Polymethylene Chain. *Spectrochim. Acta Part A Mol. Spectrosc.* **1978**, *34* (4), 395–406.

(17)    Leitner, T.; Kattner, J.; Hoffmann, H.Infrared Reflection Spectroscopy of Thin Films on Highly Oriented Pyrolytic Graphite. *Appl. Spectrosc.* **2003**, *57* (12), 1502–1509.

(18)    Coates, J.Interpretation of Infrared Spectra, a Practical Approach. *Encycl. Anal. Chem.* **2000**.

**Physical Chemistry Chemical Physics Accepted Manuscript**

(19)   Kozbial, A.; Zhou, F.; Li, Z.; Liu, H.; Li, L.Are Graphitic Surfaces Hydrophobic? *Acc.*

         *Chem. Res.* **2016**, *49* (12), 2765–2773.

(20)   Buch, V.; Devlin, J. P.*Water in Confining Geometries*; Springer Science & Business

         Media, 2013.

(21)   Hamada, I.; Otani, M.Comparative van Der Waals Density-Functional Study of Graphene

         on Metal Surfaces. *Phys. Rev. B* **2010**, *82* (15), 153412.

(22)   Hamada, I.Adsorption of Water on Graphene: A van Der Waals Density Functional Study.

         *Phys. Rev. B* **2012**, *86* (19), 195436.

(23)   Teschke, O.Imaging Ice-like Structures Formed on HOPG at Room Temperature.

         *Langmuir* **2010**, *26* (22), 16986–16990.

(24)   Xu, K.; Cao, P.; Heath, J. R.Graphene Visualizes the First Water Adlayers on Mica at

         Ambient Conditions. *Science (80-. ).* **2010**, *329* (5996), 1188–1191.

(25)   Fedorov, I. A.; Zhuravlev, Y. N.; Berveno, V. P.Structural and Electronic Properties of

         Perylene from First Principles Calculations. *J. Chem. Phys.* **2013**, *138* (9), 03B605.

(26)   Ondarçuhu, T.; Thomas, V.; Nuñez, M.; Dujardin, E.; Rahman, A.; Black, C. T.; Checco,

         A.Wettability of Partially Suspended Graphene. *Sci. Rep.* **2016**, *6*, 24237.

(27)   Lee, K.; Murray, É. D.; Kong, L.; Lundqvist, B. I.; Langreth, D. C.Higher-Accuracy van

         Der Waals Density Functional. *Phys. Rev. B* **2010**, *82* (8), 81101.

(28)   Joud, J.-C.; Houmard, M.; Berthome, G.Surface Charges of Oxides and Wettability:

         Application to TiO2–SiO2 Composite Films. *Appl. Surf. Sci.* **2013**, *287*, 37–45.

(29)   AlMahri, M. A.; Alshehhi, M.; Olukan, T.; Vargas, M. R.; Molini, A.; Alhassan, S.;

Chiesa, M.Surface Alteration of Calcite: Interpreting Macroscopic Observations by Means

of AFM. *Phys. Chem. Chem. Phys.* **2017**, *19* (37), 25634–25642.

(30)   Wang, Z.; Shi, F.; Zhao, C.Humidity-Accelerated Spreading of Ionic Liquids on a Mica

Surface. *RSC Adv.* **2017**, *7* (68), 42718–42724.

(31)   Sheppard, D.; Terrell, R.; Henkelman, G.Optimization Methods for Finding Minimum

Energy Paths. *J. Chem. Phys.* **2008**, *128* (13), 134106.

(32)   Bechstein, R.; González, C.; Schütte, J.; Jelínek, P.; Pérez, R.; Kühnle, A.'All-

Inclusive'Imaging of the Rutile TiO2 (110) Surface Using NC-AFM. *Nanotechnology*

**2009**, *20* (50), 505703.

(33)   Ondráček, M.; Pou, P.; Rozsíval, V.; González, C.; Jelínek, P.; Pérez, R.Forces and

Currents in Carbon Nanostructures: Are We Imaging Atoms? *Phys. Rev. Lett.* **2011**, *106*

(17), 176101.

(34)   Sedin, D. L.; Rowlen, K. L.Adhesion Forces Measured by Atomic Force Microscopy in

Humid Air. *Anal. Chem.* **2000**, *72* (10), 2183–2189.

(35)   San Paulo, A.; Garcia, R.Unifying Theory of Tapping-Mode Atomic-Force Microscopy.

*Phys. Rev. B* **2002**, *66* (4), 41406.

(36)   Amadei, C. A.; Santos, S.; Pehkonen, S. O.; Verdaguer, A.; Chiesa, M.Minimal

Invasiveness and Spectroscopy-like Footprints for the Characterization of Heterogeneous

Nanoscale Wetting in Ambient Conditions. *J. Phys. Chem. C* **2013**, *117* (40), 20819–

20825.

(37)   Katan, A. J.; VanEs, M. H.; Oosterkamp, T. H.Quantitative Force versus Distance

Measurements in Amplitude Modulation AFM: A Novel Force Inversion Technique.

*Nanotechnology* **2009**, *20* (16), 165703.

(38)   Tang, T.-C.; Amadei, C. A.; Thomson, N. H.; Chiesa, M.Ion Exchange and DNA

Molecular Dip Sticks: Studying the Nanoscale Surface Wetting of Muscovite Mica. *J.

Phys. Chem. C* **2014**, *118* (9), 4695–4701.

(39)   Santos, S.; Guang, L.; Souier, T.; Gadelrab, K.; Chiesa, M.; Thomson, N. H.A Method to

Provide Rapid in Situ Determination of Tip Radius in Dynamic Atomic Force Microscopy.

*Rev. Sci. Instrum.* **2012**, *83* (4), 43707.

(40)   Monkhorst, H. J.; Pack, J. D.Special Points for Brillouin-Zone Integrations. *Phys. Rev. B*

**1976**, *13* (12), 5188.

(41)   Ernzerhof, M.; Scuseria, G. E.Assessment of the Perdew–Burke–Ernzerhof Exchange-

Correlation Functional. *J. Chem. Phys.* **1999**, *110* (11), 5029–5036.

(42)   Thanthiriwatte, K. S.; Hohenstein, E. G.; Burns, L. A.; Sherrill, C. D.Assessment of the

Performance of DFT and DFT-D Methods for Describing Distance Dependence of

Hydrogen-Bonded Interactions. *J. Chem. Theory Comput.* **2010**, *7* (1), 88–96.